Assessing the photocatalytic transformation of norfloxacin by BiOBr/iron oxides hybrid photocatalyst: Kinetics, intermediates, and influencing factors

Changsheng Guo [a], Shengwang Gao [a,b], Jiapei Lv [a], Song Hou [a], Yuan Zhang [a], Jian Xu [a,*]

[a] State Key Laboratory of Environmental Criteria and Risk Assessment, Chinese Research Academy of Environmental Sciences, Beijing 100012, China
[b] Department of Chemistry, College of Science, North University of China, Taiyuan 030051, China

ABSTRACT

Norfloxacin (NOR) is a widely used fluoroquinolone antibacterial that has drawn much concern due to its adverse effect on aquatic ecology and human health. In this study, a novel magnetically recoverable BiOBr/iron oxides (BiOBr/Fe$_3$O$_4$) heterojunction photocatalyst with high photocatalytic activity on NOR was successfully synthesized using a facile *in-situ* coprecipitation method. The samples were characterized by X-ray diffraction, transmission electron microscopy, X-ray photoelectron spectroscopy, UV–vis diffuse reflectance spectra, N$_2$ adsorption-desorption analysis, and vibrating sample magnetometer. Several factors affecting the catalytic performance of BiOBr/Fe$_3$O$_4$ were investigated. Results showed that the catalytic degradation efficiency of NOR increased with the increasing bicarbonate doses, but decreased with the increasing natural organic matter concentrations. The presence of nitrate stimulated NOR degradation by BiOBr/Fe3O4 at low concentrations but inhibited the degradation at high concentrations. The photogenerated reactive species were determined based on free radicals trapping experiments, revealing that the photodegradation of NOR over BiOBr/Fe3O4 under visible light was dominated by superoxide radicals and hydroxyl radicals rather than oxidation by direct holes. On the basis of the degradation products identified by HPLC–MS, the NOR degradation pathway was proposed. NOR possibly underwent the piperazine ring transformation, decarboxylation and defluorination to generate eleven intermediates. Toxicity assays by Vibrio fischeri proved that the NOR photocatalytic transformation products retained negligible antibacterial activity relative to the parent compound. The catalytic degradation of NOR by BiOBr/Fe3O4 was also effective in the actual natural waters.

© 2016 Elsevier B.V. All rights reserved.

1. Introduction

The presence of pharmaceutical compounds in the aquatic environment and their potential adverse effects have drawn increasing concern because a majority of these compounds cannot be eliminated in conventional wastewater treatment plants (WWTPs). Current drinking water standards do not even require testing for prescribed pharmaceutical compounds. Pharmaceutically active compounds such as antibiotics, analgesics, steroids, hormones, etc., have been detected in various water bodies around the world [1–3]. In particular, the occurrence and fate of antibiotic pharmaceuticals in municipal WWTPs is currently a subject of rapidly increasing interest to both scientists and water quality regulators.

Fluoroquinolones (FQs) are a class of synthetic antibacterials with broad-spectrum antibiotic properties by inhibiting DNA replication and transcription. Their high effectiveness has made them widely used both in human medicine and veterinary practice [4]. However, most fluoroquinolones are not fully metabolized in the body and more than 50% of their parent active form may be excreted directly into the environment. They are poorly biodegraded and will end up in the wastewater treatment effluent [5,6].

Norfloxacin (NOR) is the second generation of synthetic fluoroquinolone used for treating urinary tract infections. It has been frequently detected in the aquatic systems, including sewage treatment plants [2,4,7], surface water [1,2,8], ground water and drinking water [1,9,10]. Previous studies verified that NOR was toxic to plants [11] and aquatic organisms [12]. It could also induce irreversible adverse effects and threaten the ecosystem function by increasing the resistance of bacteria against drugs [12] and spreading the antibiotic resistance genes among bacterial populations. It is

therefore necessary and significant to develop effective techniques to remove NOR from the contaminated environment.

In the past decades, some biological and non-biological techniques, including bacterial or fungal degradation, sorption, hydrolysis, photolysis, oxidation and reduction have been applied for NOR removal, however, these techniques could not completely eliminate NOR from the environmental matrices [6,13]. Photocatalytic degradation has been considered as a promising technique for the degradation of organic pollutants, because the nano-sized photocatalysts could generate highly reactive oxidative radicals capable of degrading those biorefractory contaminants effectively [6,8]. Researchers examined the photocatalytic degradation of NOR in aqueous systems by different photocatalysts, such as δ-MnO_2 [14], TiO_2 [5], SnS_2 [15], C-TiO_2 [16] and Bi_2WO_6 [6,17]. One disadvantage of the above nanoparticles in the practical application was their recovery from solutions. Developing the magnetic photocatalysts has proved to be an easy technique to overcome this difficulty. The synthesized composite composing of both catalyst with high photocatalytic performance and magnetic material enabled its easily recovery ability by a magnet. Among the catalysts, bismuth oxyhalides (BiOX, X = I, Br, Cl) were a family of promising photocatalysts with special electronic structures and excellent photocatalytic performance under visible light irradiation. A few studies reported the preparation of Fe_3O_4 and bismuth oxyhalides (BiOX, X = Cl, I) heterojunction structures for the application of dyes removal [18,19]. To our best knowledge, no study was conducted on photocatalytic degradation of antibiotic norfloxacin using the solar-light mediated BiOBr/Fe_3O_4 nanocomposite.

In this study, a BiOBr/Fe_3O_4 nanocomposite was prepared by a facile in-situ co-precipitation method. The synthetic BiOBr/Fe_3O_4 was employed to degrade NOR in a heterogeneous reaction system, and the effect of various parameters including solution pH, the water matrix, electron receptors, dissolved organic matter (DOM) and inorganic salts on the kinetics of degradation was evaluated. The degradation intermediates and products were identified as well, and a tentative transformation pathway was proposed. A toxicity assays by *Vibrio fischeri* was also conducted to investigate the toxicity evolvement of the degradation process.

2. Materials and methods

2.1. Chemicals and reagents

Norfloxacin (purity > 99%) was purchased from Sigma-Aldrich (St. Louis, MO, USA). Bismuth nitrate pentahydrate (Bi(NO$_3$)$_3$·5H$_2$O), ferrous sulfate (FeSO$_4$·7H$_2$O), sodium acetate (NaAc) and potassium bromide (KBr) were purchased from Sinopharm Chemical Reagent Co., Ltd. (SCRC, Shanghai, China). Methanol and acetonitrile (HPLC grade) were obtained from Merck (Darmstadt, Germany). All other reagents were of analytical grade, which were purchased from Tianjin Chemical Reagents Company (Tianjin, China) and used without further purification. Milli-Q (MQ) ultrapure water was produced via a purification system (Millipore, Bedford, MA, USA).

2.2. Preparation of BiOBr/Fe$_3$O$_4$

BiOBr/Fe_3O_4 was prepared by the chemical coprecipitation method. An amount of 1 mmol of $C_6H_5Na_3O_7$·$2H_2O$ (sodium citrate tribasic dihydrate), 4 mmol of NaOH, and 0.2 mol of $NaNO_3$ were mixed in 19 mL of deionized water. The mixture was heated to 100 °C forming a pellucid solution. An aliquot of 1 mL of 2 M FeSO$_4$·4H$_2$O (2 mmol) solution was added into the mixture quickly, and the mixed solution was kept at 100 °C for 1 h. The solution was naturally cooled down to room temperature. The Fe_3O_4

nanoparticles were separated from the solution with a magnet, washed by deionized water and ethanol for several times, and dried at 60 °C for 6 h. To synthesize heterostructured BiOBr/Fe_3O_4 photocatalyst, 2.0 mmol of bismuth nitrate pentahydrate (Bi(NO$_3$)$_3$·5H$_2$O) were dissolved in 5 mL glacier acetic acid. The resulting solution was added dropwise to 100 mL solution which contained 2 mmol KBr, 3.0 mol CH_3COONa and 2.0 mmol Fe_3O_4 nanoparticles. The mixture was vigorously stirred for 3 h. The powder was collected and rinsed thoroughly with distilled water and absolute ethanol, and dried at 60 °C for 6 h.

2.3. Characterization

The phase identification of synthesized BiOBr/Fe_3O_4 was conducted by a Rigaku D/Max-2500 diffractometer using Cu Kα radiation (λ = 0.154178 nm). The morphology and size were examined by transmission electron microscopy (TEM, JEM-100CXII). Surface element compositions were analyzed by a Kratos Axis Ultra DLD multi-technique X-ray photoelectron spectroscopy (XPS) with a monochromated Al Kα X-ray source. Magnetic properties were obtained using a vibrating sample magnetometer (VSM, LDJ9600). The N_2 adsorption-desorption measurements were carried out on a Quantachrome NOVA 2000e automatic analyzer at 77 K. UV–vis diffuse reflectance spectra was performed with a UV–vis spectrophotometer using $BaSO_4$ as the reference in the range of 200–800 nm (Shimadzu, UV-3600).

2.4. Photocatalytic degradation experiments

Photochemical experiments were conducted in a photochemical reactor at ambient temperature, with detailed operating conditions reported previously [20,21]. An 800 W xenon lamp (Institute of Electric Light Source, Beijing) which was positioned in the cylindrical quartz trap and surrounded by circulating water was used as the light source with a 420 nm cutoff filter to provide visible light irradiation. The pH was adjusted with 1 M HCl or NaOH. For all degradation kinetics studies, each experiment was conducted in triplicate and beyond one degradation half-life. A quantity of 0.05 g of BiOBr/Fe_3O_4 catalyst was added into 50 mL NOR solution. Prior to irradiation, the suspension was stirred in darkness for 30 min to achieve adsorption-desorption equilibrium of NOR on BiOBr/Fe_3O_4 (a preliminary study indicated that 30 min was sufficient to achieve adsorption equilibrium). After a given irradiation time, an aliquot of 200 μL reaction solution was withdrawn. The solution was separated by an external magnetic field, and filtered through 0.45 μm nylon membrane prior to NOR analysis. All the experiments were conducted in triplicate and error bar represented the standard deviation of the replicate experimental data.

2.5. Products identification

An Agilent 1200 series HPLC equipped with a ZORBAX Eclipse XDB-C18 column (100 mm × 2.1 mm, 5 μm thickness, Agilent, USA) with ultraviolet detector (emission wavelength at 272 nm) was used to determine NOR concentration. The ratio of mobile phase of eluent A (0.1% formic acid in ultrapure water) to eluent B (methanol) was 30:70 (v/v). The flow rate was 0.2 mL/min and the injection volume was 10 μL. The column was maintained at 30 °C during the sample analysis.

The products/intermediates were detected using a Thermo LCQ Advantages instrument (Quest LCQ Duo, USA) equipped with an electrospray ionization (ESI) source and operated in the positive electronspray ionization mode (ESI+). The capillary voltage and cone voltage were set at 3.5 kV and 25 V, respectively. The desolvation temperature and source temperature were at 350 °C and 120 °C, respectively. Chromatographic separation of these
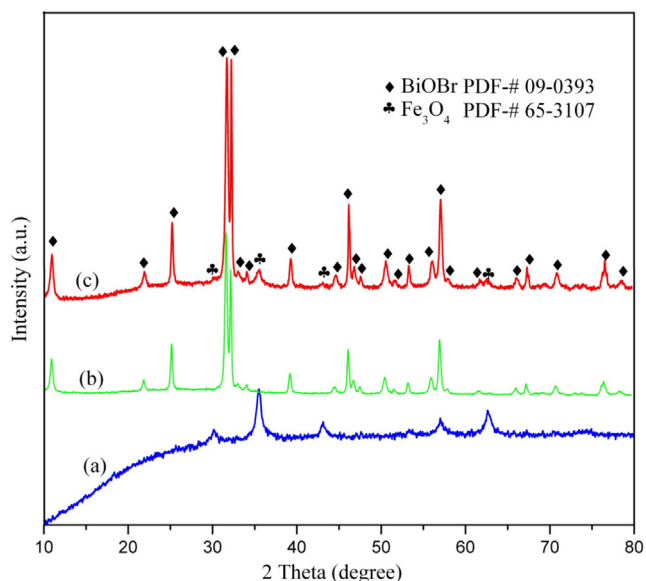
Fig. 1. XRD patterns of (a) Fe_3O_4 NPs, (b) BiOBr nanosheets, and (c) BiOBr/Fe_3O_4 nanocomposites.

products was performed using an Agilent 1200 module (Agilent, Palo Alto, CA, USA) equipped with a ZORBAX Eclipse XDB-C18 column (100 mm × 2.1 mm, 5 μm thickness, Agilent, USA). Mobile phase A was 0.1% formic acid (v/v) in ultrapure water, and mobile phase B was methanol. The separation of the intermediates was conducted with the following gradient program: 0–5 min: 10% B; 5–7 min: 10–15% B; 7–11 min: 15–40% B; 11–15 min: 40–90% B; 15–20 min: 90% B; 20–25 min: 90–10% B. The sample injection volume was 20 μL. The system was re-equilibrated for 10 min between runs.

2.6. Toxicity measurement

The bioluminescence inhibition assay was conducted to monitor the toxicity of an unirradiated NOR solution and the toxicity variation during the NOR photocatalytic degradation. *Vibrio fischeri* was selected as the luminescent bacteria, and the toxicity was measured with a Microtox Model 500 Toxicity Analyzer. The initial NOR concentration was set at 10 mg L^{-1}, the same as those in products identification studies. Freeze-dried bacteria, reconstitution solution, diluent (2% NaCl) and an adjustment solution (non-toxic 22% sodium chloride) were obtained from Beijing Hamamatsu (Beijing, China). Samples were examined in quartz tube containing 2% sodium chloride in three dilutions. A toxic-free control experiment in three repeats was conducted only containing 2% sodium chloride. The luminescence was recorded after 15 min of incubation at 15 °C. The percentage of luminescence inhibition was calculated according to the procedure described in the literature [22].

3. Results and discussion

3.1. Characterization of the prepared catalysts

Fig. 1a showed the XRD patterns of the Fe_3O_4 nanoparticles (NPs), BiOBr nanosheets and BiOBr/Fe_3O_4 synthesized by the simple chemical co-precipitation method. For the Fe_3O_4 NPs, the diffraction peaks at 30°, 35.4°, 43°, 53.4°, 56.9°, and 62.5° responded to (220), (311), (400), (422), (511), and (440) planes of cubic Fe_3O_4 lattice, respectively. These results were in good agreement with those XRD patterns of Fe_3O_4 NPs reported JCPDS card (no. 65–3170). No characteristic peaks belonging to impurity phases

(Fe_2O_3 or FeOOH) were observed, indicating high purity of the Fe_3O_4 NPs. The particle size of the Fe_3O_4 powders estimated using Scherrer's formula was ca. 30 nm. It was noted that all the diffraction peaks in the XRD pattern of the BiOBr powders synthesized via facile co-precipitation methods matched with that of standard XRD pattern (JCPDS card no. 09-0393) for tetragonal BiOBr phase. The diffraction peaks at 10.96°, 25.16°, 31.69°, 32.22°, 46.21°, 50.67°, 57.12° and 76.69° responded to (001), (101), (102), (110), (200), (104), (212) and (310) planes of the high purity of the prepared BiOBr catalysts. The intense and sharp diffraction peaks suggested the good crystallinity of BiOBr catalysts. The structure and morphology of the catalysts were examined by TEM and HRTEM (Fig. 2). Fig. 2a showed that the obtained Fe_3O_4 NPs were spherical with the average diameter of about 30 nm. The panoramic view shown in Fig. 2b indicated that as-synthesized BiOBr products were composed of lamellar structure. The length of the plates was between 300 nm and 500 nm. The TEM and HRTEM images of the BiOBr/Fe_3O_4 sample synthesized were shown in Fig. 2c and 2d. Close observation on the samples by the high magnification TEM image demonstrated further details of the BiOBr lamellar structure. Clearly, the morphology of the as-synthesized BiOBr/Fe_3O_4 was also composed of large lamellar structure with numerous monodispersed Fe_3O_4 NPs uniformly decorating on the BiOBr nanosheets, and lots of the pleats proved that the lamellas were ultrathin.

The surface elemental compositions and chemical states of samples were identified by XPS analysis. The peak positions in all XPS spectra depicted in Fig. S1 (supplementary data) were calibrated with C 1s at 284.8 eV. The typical survey XPS spectra of BiOBr/Fe_3O_4 indicated the existence of Fe, O, Bi, and Br elements. As shown in Fig. S1b, the peak at 159.5 eV and 164.8 eV was assigned to Bi $4f_{7/2}$ and Bi $4f_{5/2}$, respectively, which was attributed to the characteristic of Bi^{3+} in BiOBr. The peak of Br 3d at 68.7 eV was attributed to Br element (Fig. S1c). The peaks in Fig. S1d at 711.0 eV and 724.5 eV were determined to be Fe $2p_{3/2}$ and Fe $2p_{1/2}$, respectively. Previous reports indicated that there was no satellite peak on Fe $2p_{3/2}$ for Fe_3O_4 [23]. The absence of the satellite peak were proved in Fig. S1d, confirming the Fe^{2+} and Fe^{3+} were included in Fe_3O_4. The peaks of O 1s at 530.5 eV and 529.7 eV were ascribed to Bi—O and Fe—O bonds, respectively (Fig. S1e). The binding energy at 531.9 eV was assigned to the hydroxyl anion on the surface adsorption of water. The above analysis result revealed the composites consisted of BiOBr and Fe_3O_4, which was also consistent with the XRD analysis.

Fig. S2 showed the room-temperature magnetic hysteresis loops of the as-synthesized samples. The samples exhibited typical ferromagnetic behavior. The saturation magnetization saturation (Ms) values for the Fe_3O_4 NPs and BiOBr/Fe_3O_4 nanocomposites were 52.4 and 47.5 emu/g, respectively. It was noteworthy that the Ms values of BiOBr/Fe_3O_4 nanocomposites were much lower than that of the Fe_3O_4 NPs, which was ascribed to the existence of nonmagnetic BiOBr in the total mass. As the content of Fe_3O_4 nanoparticles decreased, the saturation magnetization decreased, which was in good agreement with previous reports [24]. The remanence (Mr) and coercivity (Hc) were 0.8 emu/g and 6.7 Oe for Fe_3O_4 NPs, and 0.7 emu/g and 6.4 Oe for BiOBr/Fe_3O_4 respectively. Given the small remanence and coercivity, the Fe_3O_4 NPs and BiOBr/Fe_3O_4 nanocomposites exhibited superparamagnetic behavior. Strong magnetization of the heterostructured BiOBr/Fe_3O_4 photocatalysts allowed them to be rapidly and conveniently separated from an aqueous solution by applying an external magnetic field. The magnetic separability of the as-obtained nanocomposites was tested in water by placing a magnet near the glass bottle. The samples were completely attracted to a magnet within 30 s and the solution became transparent (the upper inset in Fig. S2). The results clearly illustrated the quickly magnetic response of multifunctional hybrid nanocomposites.
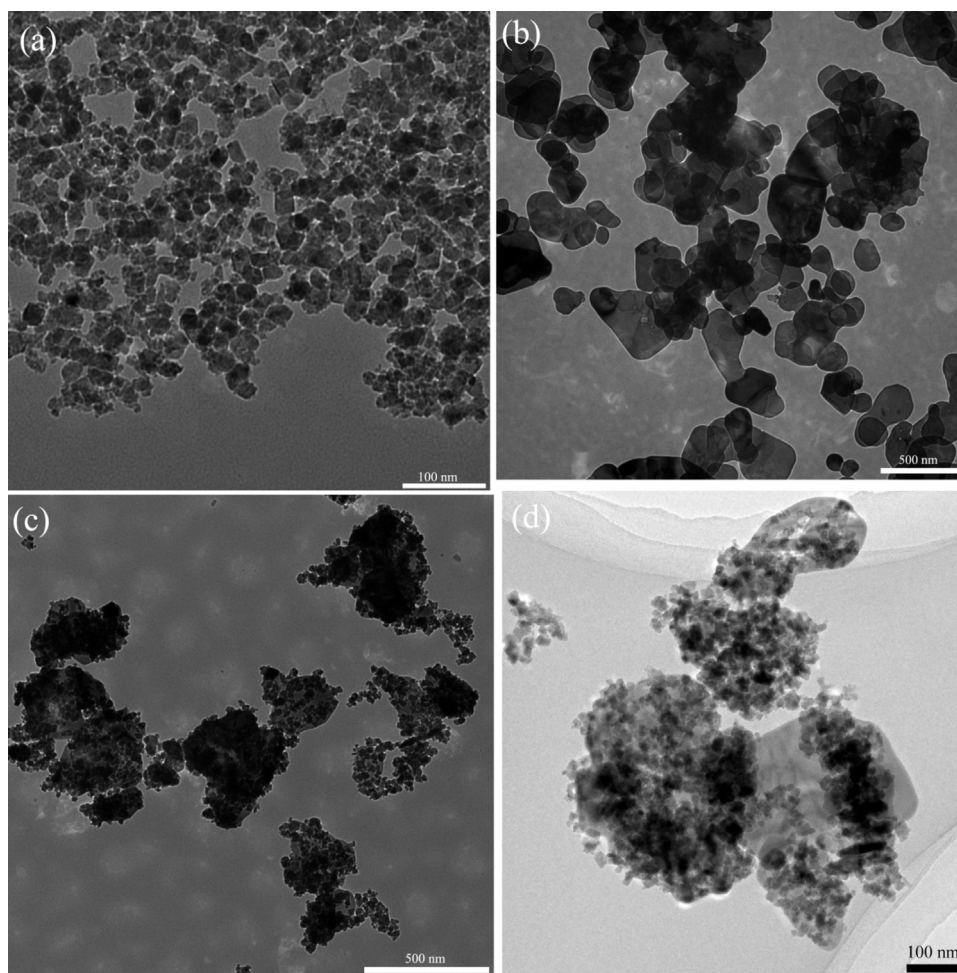
Fig. 2. TEM images (a) Fe_3O_4, (b) BiOBr, (c) BiOBr/Fe_3O_4 and HRTEM (d) BiOBr/Fe_3O_4 of the synthesized samples.

The specific surface area and porosity of the prepared samples were presented in Fig. S3. The isotherms of the samples showed a type IV with a hysteresis loop, suggesting the as-prepared sample could be identified as mesoporous materials. The specific surface area of BiOBr/Fe_3O_4 was 30.85 $m^2\,g^{-1}$, larger than that of BiOBr (12.31 $m^2\,g^{-1}$). The pore volumes of the BiOBr and BiOBr/Fe_3O_4 composites were 0.095 $cm^3\,g^{-1}$ and 0.047 $cm^3\,g^{-1}$, respectively, which meant there were a few small pores on the surface of composites. The opened channels would not only allow the reactants to enter the spheres, but also improve the mass transfer within the hybrid structure during photocatalytic process [21].

UV–vis diffuse reflectance spectra of the as-synthesized photocatalysts were displayed in Fig. S4. It showed that the absorption edge of BiOBr at 436 nm was weak for visible light while the absorption edge of BiOBr/Fe_3O_4 was extended to 688 nm. Compared to BiOBr, the absorption edges of BiOBr/Fe_3O_4 had a remarkable red shift with the introduction of Fe_3O_4. The band gap energy of the samples was calculated according to the formula: $\alpha h\nu = A\,(h\nu\text{-}E_g)^{n/2}$, where α, ν, E_g and A were the absorption coefficient, light frequency, band gap, and a constant, respectively. Herein, the value of n was 4 for BiOBr due to their indirect transition [21,25]. The E_g of the as-prepared samples can be estimated from a plot of $(\alpha h\nu)^{1/2}$ versus energy ($h\nu$). As shown in Fig. S4b, the band gap of BiOBr was 2.63. The E_g of BiOBr/Fe_3O_4 samples was 1.94 eV. The lower energies of the composites suggested an enhanced absorption in the visible region compared to BiOBr, which was likely due to the incorporation of Fe_3O_4 NPs to the BiOBr photocatalyst. These results suggested that the coupled heterostructures were more effective in absorbing visible light that would profitably enhance the photocatalytic activity under visible light irradiation.

3.2. Photocatalytic degradation of NOR

3.2.1. Role of pH

The UV–vis absorption spectrum was run for NOR at pH range 3–11. The compound was found to absorb light at wavelengths >268 nm (Fig. S5). Prior to the experiment, NOR solution of 10 mg/L was continuously stirred for 1 h in the dark without adding the photocatalyst. No obvious concentration changes were observed, indicating that the hydrolysis of NOR under dark is negligible. Additionally, preliminary study showed that adsorption of NOR on catalysts was less than 4% (Fig. S6) without irradiation, suggesting that NOR removal due to adsorption was minimal and photocatalytic degradation was the main contributor to NOR removal. The conversion and rate constant of NOR degradation at various pH values were given in Fig. 3. The photocatalytic degradation of NOR depended strongly on the pH of the solution and was substantially reinforced at neutral and weak alkaline conditions (pH 7–9), while was hindered at strongly alkaline (pH > 10) and acidic conditions (pH < 6). The degradation could be well described by first-order reaction kinetics at various pH values. The rate constant k values were shown in inset of Fig. 3. The highest k value in water was 0.073 and 0.076 min^{-1} at pH 7 and pH 9, respectively, apparently exceeding the maximal rate (0.026, 0.046 and 0.027 min^{-1}) at pH 3, 5 and 11. The interpretation of the pH effects on the efficiency of NOR photocatalytic degradation process was complicated due
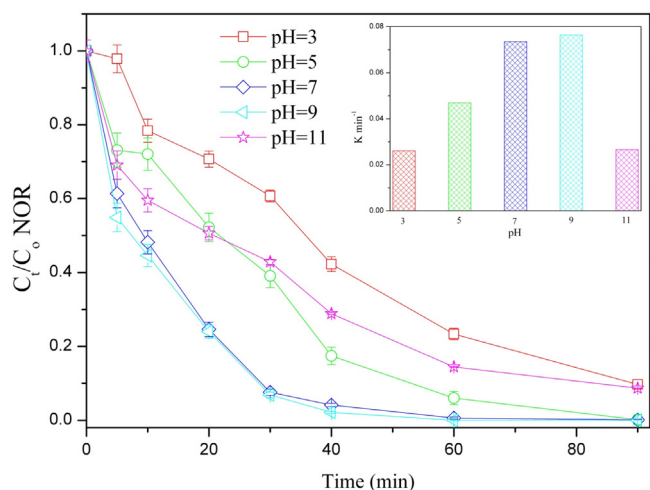
Fig. 3. The photocatalytic degradation of NOR by the prepared materials at different pH values under the visible light irradiation and their pseudo first-order rate constants (inset).
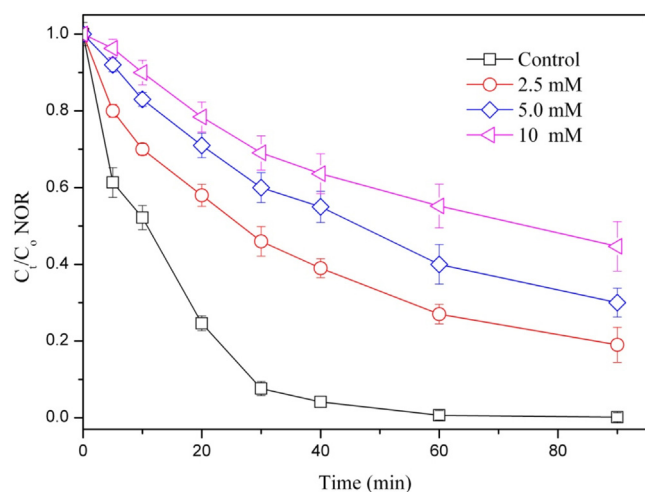

Fig. 5. Influence of nitrate on NOR degradation by BiOBr/Fe$_3$O$_4$. Conditions: photocatalyst, 0.5 g L^{-1}; NOR, 10 mg L^{-1}, pH = 7.3 ± 0.2.

the BiOBr/Fe$_3$O$_4$ system, NOR degradation was inhibited by the addition of HA. The degradation efficiency at 90 min decreased from 99.8% to 81.3%, 70.5% and 55.31% when DOM concentration increased from 0 mM to 2.5 mM, 5 mM and 10 mM (Fig. 4). It indicated that the stimulated effect of DOM was overwhelmed by its detrimental effect in the range of 2.5–10 mM.

As shown in Fig. S7, HA absorbed UV–vis from 200 to 700 nm. The inhibition effect of HA was probably due to the competitive absorption of short-wavelength photons under UV–vis irradiation (λ > 200 nm) since HA could absorb more UV than visible light and •OH was of no help to NOR photocatalytic degradation. Although HA could also enhance the photodegradation as a photosensitizer [27–29], the result of this experiment indicated that photosensitization might be secondary to the NOR degradation. This was corresponded with previous studies that HA could bring about light attenuation [30,31].

3.2.3. Effect of nitrate

Nitrate under solar light was the major precursor for •OH [8,32]; it was commonly present in surface waters and ranged in concentrations from 10^{-5} to 10^{-3} M. As shown in Fig. 5, NO$_3^-$ enhanced the degradation of NOR slightly at low concentration (<1.0 mM), and they inhibited the reaction slightly in the concentration range of 2.0–10.0 mM. The photolysis of NO$_3^-$ could produce •OH, which was a strong oxidant and could oxidize many organic chemicals non-selectively [33]. Hydroxyl radical could contribute to the oxidation and degradation for NOR in this sysytem. However, excessive nitrate (>2.0 mM) would lead to reducing for the NOR removal efficiency. The excessive NO$_3^-$ ions could be adsorbed on the catalyst and compete for the active sites on the catalyst surface with NOR, thus inhibited the photocatalytic activity for NOR degradation.

3.2.4. Effect of bicarbonate

Bicarbonate anion was a radical scavenger, and reaction between •OH and either carbonate or bicarbonate ion was conductive to the formation of carbonate radicals •CO$_3^-$ which was more selective and less reactive than •OH, and could easily result in the degradation of easily oxidized organic substances [34]. The overall effect of bicarbonate on the indirect photocatalytic degradation rates seemed to be compound-specific. The presence of bicarbonate had been reported to slightly inhibit the photolysis of pharmaceuticals and pesticides in a nitrate system [8,35]. However, many other studies also demonstrated bicarbonate-enhanced photodegradation of cephalosporins, 4-halogenophenols, thioanisole,

Fig. 4. Influence of DOM on NOR degradation by BiOBr/Fe$_3$O$_4$. Conditions: photocatalyst, 0.5 g L^{-1}; NOR, 10 mg L^{-1}, pH = 7.3 ± 0.2.

to the multiple roles. The ionization states of the catalyst surface and the substrate, as well as the rate on the formation of radicals and other reactive species in the reaction mixture [25,26] could attribute to the degradation. According to Fig. S5, NOR had the pKa1 and pKa2 values of 6.34 and 8.75. In this respect, under neutral or alkaline conditions hydroxyl radicals were easily generated by the oxidation of the hydroxide ions which were available on the BiOBr/Fe$_3$O$_4$ surface and therefore the efficiency of the process was enhanced. In addition, at high pH values the hydroxyl radicals were rapidly scavenged and they did not have the opportunity to react with organic compounds [26].

3.2.2. Effect of DOM

DOM as an important water constituent played important roles in the transfer and transformation of water borne chemicals under light irradiation. DOM could progress through an excited triplet state (e.g., ^{3}DOM*) to form excited species (e.g., singlet oxygen (^{1}O$_2$), peroxyl radicals (ROO•)), and aqueous electrons (e$_{aq}^-$) that photooxidize organic contaminants. On the other hand, DOM could also react with and serve as the sink for these excited species. The effect of humic acid (HA, representing DOM in this study) on the NOR photocatalytic degradation was shown in Fig. 4. In
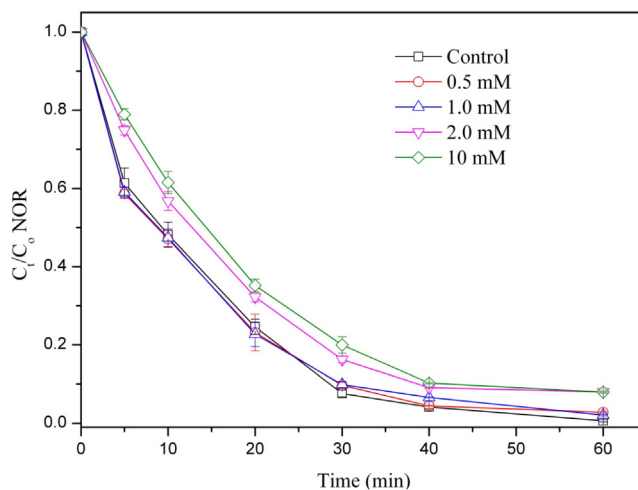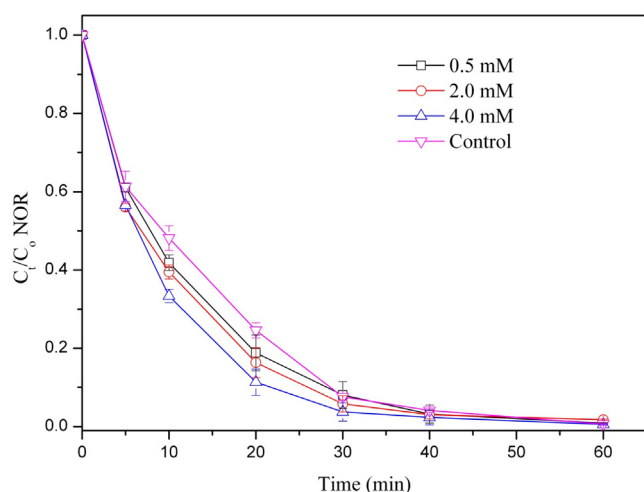
Fig. 6. Effect of bicarbonate on NOR degradation by BiOBr/Fe$_3$O$_4$. Conditions: photocatalyst, $0.5\,g\,L^{-1}$; NOR, $10\,mg\,L^{-1}$, pH = 7.3 ± 0.2.

Fig. 7. Photocatalytic degradation kinetics of NOR and $0.5\,g\,L^{-1}$ BiOBr/Fe$_3$O$_4$ in the presence of various scavengers: 0.1 M isopropanol, 0.1 M KI, 0.1 M BQ, 0.1 M NaN$_3$, and in pure methanol.

fenthion, dibenzothiophere, and *N,N*-dimethylaniline in the presence of nitrate [8,36,37].

In the BiOBr/Fe$_3$O$_4$ system, bicarbonate enhanced NOR degradation at the concentration from 0.5 to 4 mM as shown in Fig. 6. Vione et al. reported that bicarbonate enhanced the photolysis of compounds that were sufficiently reactive toward the $^\bullet CO_3^-$ [36]. Studies showed that carbonate radical reacted rapidly with compounds bearing easily oxidizable moieties, such as amino acids and aromatic anilines bearing electron-donating substituents [8]. The carbonate radical may also be a significant reactant in the oxidation of sulfur-containing compounds [8,34]. NOR had structures similar to amino acids, and had two aromatic aniline's structure. The complexes of bicarbonate on BiOBr/Fe$_3$O$_4$ surface might also be a reason for the degradation enhancement. This may explain the rapid photocatalytic oxidation rates ($t_{1/2}$ = 7.9 min, 4.0 mM bicarbonate) observed for NOR.

3.3. Reactive species and possible mechanism

3.3.1. Reactive species

In the photocatalytic processes, a series of oxidative or reductive species, such as h$^+$ and e$^-$ aq, as well as $^\bullet$OH, $^\bullet O_2^-$, and $^1O_2$, could be produced that reacted with NOR. Both oxidative (for instance, $^\bullet$OH) and reductive species (for instance, e$^-$ aq) could rapidly react with NOR, but the contribution from each species was still unclear. The photocatalytic degradation kinetics of NOR with or without specific scavengers, therefore, were conducted to distinguish the main reactive species involved. Isopropanol was used to scavenge $^\bullet$OH [20], methanol was used to remove the contribution of h$^+$ and $^\bullet$OH [38], KI was used to remove h$^+$ and surface $^\bullet$OH [14], benzoquinone (BQ) was used to remove $^\bullet O_2^-$ [25], and sodium azide (NaN$_3$) was used to rule out the participation of $^1O_2$ [31]. The degradation kinetics was depicted in Fig. 7, and the variation of pseudo-first-order rate constants under different conditions was also summarized in Fig. S8.

Without any scavengers, the rate constant k was 0.0837 min^{-1} in the reaction system, The k value decreased to 0.0056 min^{-1} when $^\bullet$OH was removed by isopropanol, indicating 93.2% of NOR degradation was attributed by $^\bullet$OH. With the reaction in methanol, the rate constant decreased notably to 0.0024 min^{-1}, suggesting that both $^\bullet$OH and h$^+$ contributed 97.2% of the NOR removal. This result indicated that h$^+$ also engaged in photocatalytic degradation of NOR probably by direct electron transfer process, but only contributed 4.0% of the NOR removal. The rate constant reduced to
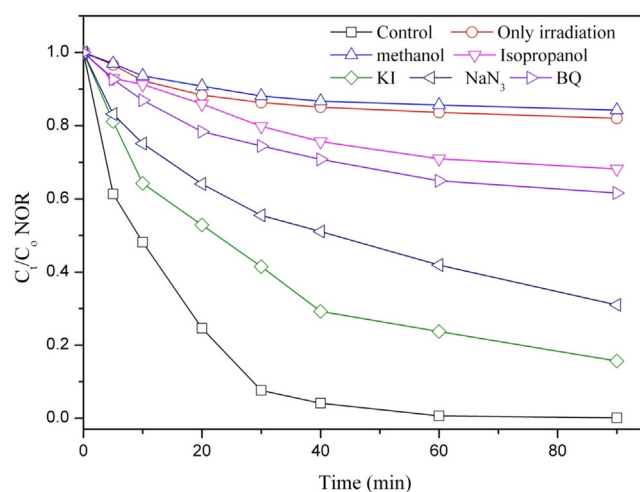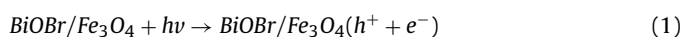
0.0245 min^{-1} (by 70.7%) in the presence of KI, further suggesting that NOR degradation was mostly induced by $^\bullet$OH.

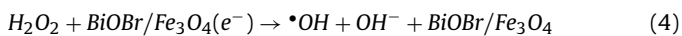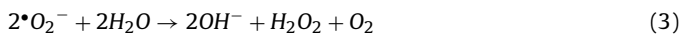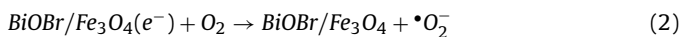The rate constant decreased obviously to 0.00698 min^{-1}, in the presence of BQ [39], which suggested that $^\bullet O_2^-$ was also the main reactive species for the degradation of NOR in the BiOBr/Fe$_3$O$_4$ system. The generation of $^\bullet O_2^-$ could be via photoinduced electrons reacting directly with O$_2$ adsorbed on the surface of the catalyst [18]. NOR could be excited under visible light irradiation, and the excited NOR injected electrons into the conduction band of BiOBr/Fe$_3$O$_4$ via electron transfer to generate conduction electrons, which were captured by O$_2$ molecules to form $^\bullet O_2^-$ radicals. These $^\bullet O_2^-$ radicals could react with the radical cations leading to the degradation of NOR. The rate constant was obtained at 0.0137 min^{-1} in the presence of NaN$_3$. This may be caused by NaN$_3$ molecules that hindered the NOR adsorption and light irradiation on the surface of the BiOBr/Fe$_3$O$_4$ catalysts, resulting in a decrease of the degradation rate. The results showed that $^1O_2$ did not play significant role in the degradation of NOR.

To further study the radicals generated in the photocatalytic system under visible irradiation and confirm the NOR degradation mechanism, the ESR spintrap with DMPO technique was carried out on the BiOBr/Fe$_3$O$_4$ heterojunction photocatalyst at room temperature. Both of the ESR signals intensities were quite week when there was no light irradiation, suggesting that the BiOBr/Fe$_3$O$_4$ photocatalyst did not generate $^\bullet$OH and $^\bullet O_2^-$ in the dark. As shown in Fig. S9, the characteristic signals of the DMPO-$^\bullet O_2^-$ were observed for BiOBr/Fe$_3$O$_4$ under light irradiation, suggesting that $^\bullet O_2^-$ can be generated efficiently via the single electron transfer process. Meanwhile, a 4-fold characteristic peak with an intensity ratio of 1:2:2:1 was observed for DMPO-$^\bullet$OH adduct, revealing the $^\bullet$OH could also be generated by BiOBr/Fe$_3$O$_4$ (Fig. S9b). It was well recognized that $^\bullet$OH and $^\bullet O_2^-$ could be produced during the photocatalytic process and played important role in the degradation of NOR.

3.3.2. Photocatalytic degradation mechanism

In general, four possible reaction mechanisms should be considered for the NOR degradation, the photoabsorption of the semiconductor catalyst, the generation of photogenerated electron and hole, the transfer of charge carriers, and the utilization of the charge carriers by the reactants [25,39]. According to the above experimental results and analyses, a possible photocatalytic pathway of the BiOBr/Fe$_3$O$_4$ nanocomposites was proposed as follows.

$$BiOBr/Fe_3O_4 + h\nu \rightarrow BiOBr/Fe_3O_4(h^+ + e^-) \tag{1}$$

$$BiOBr/Fe_3O_4(e^-) + O_2 \rightarrow BiOBr/Fe_3O_4 + {}^\bullet O_2^- \qquad (2)$$

$$2{}^\bullet O_2^- + 2H_2O \rightarrow 2OH^- + H_2O_2 + O_2 \qquad (3)$$

$$H_2O_2 + BiOBr/Fe_3O_4(e^-) \rightarrow {}^\bullet OH + OH^- + BiOBr/Fe_3O_4 \qquad (4)$$

$$NOR + {}^\bullet OH, {}^\bullet O_2^-, h^+ \rightarrow products \qquad (5)$$

In Fig. 7, the NOR degradation in the blank experiment under visible light irradiation could not be observed, which meant that the NOR was stable and the photolysis process had a negligible contribution. In other words, the NOR degradation might be initiated possibly by a photocatalytic process. Fig. S10 demonstrated the TOC changes in the NOR degradation system by $BiOBr/Fe_3O_4$. After irradiation for 90 min, the TOC values of the NOR solution decreased by 14.2% in the presence of $BiOBr/Fe_3O_4$ catalysts.

In this study, the enhanced photocatalytic activity was mainly derived from the efficient generation, separation and transfer of the photo-induced electron-hole pairs, which strongly depended on the band structure of the composite photocatalyst [18,40]. BiOBr was a p-type semiconductor, whereas Fe_3O_4 was a n-type semiconductor. The formation of the *p-n* junction could lead to an efficient electron-hole separation that minimizes the recombination of photoexcited electron-hole pairs [21]. The valence bands (VB) and conduction bands (CB) of BiOBr ($E_{VB} = 2.94$ eV, $E_{CB} = 0.36$ eV) [41], and Fe_3O_4 ($E_{VB} = 0.27$ eV, $E_{CB} = 0.17$ eV) [21] were provided to clearly clarify the separation and transfer of electron-hole pairs at the interface of the heterostructures. As shown in Fig. 8, once the electrons in the VB of Fe_3O_4 and BiOBr were excited to the CB under irradiation, the photo-induced electrons on the CB of Fe_3O_4 would transfer to the CB of BiOBr while the photogenerated holes on the VB of BiOBr would transfer to the VB of Fe_3O_4 [18,21,41]. These resulted in the gathering of large number of electrons on the CB of BiOBr surface and holes on the VB of Fe_3O_4 (Eq. (1)). Consequently, the photo-induced electrons and holes were separated efficiently and their recombination decreased. After that, electrons reacted with O_2 adsorbed on the surface of catalyst to generate reactive ${}^\bullet O_2^-$ (Eq. (2)) that induced the degradation of NOR (Eq. (5)). Meanwhile, further reaction with the O_2 via two-electron reduction process (Eq. (3)) would finally generate reactive ${}^\bullet OH$ (Eq. (4)) that induced the degradation of NOR (Eq. (5)). Through this way, the photogenerated carriers could be separated efficiently and improve the photocatalytic activities of $BiOBr/Fe_3O_4$. The schematic diagrams of the band configuration and charge separation were illustrated in Fig. 8.

3.4. Stability of the photocatalysts

The stability of a catalyst was regarded as a critical property in the large-scale application. The stability of the $BiOBr/Fe_3O_4$ photocatalyst was evaluated by several recycling runs. As shown in Fig. 9a, after six recycles for the photogradation of NOR, photocatalytic performance of $BiOBr/Fe_3O_4$ maintained well, only with small loss of the activity.

The structural stability of $BiOBr/Fe_3O_4$ was also investigated by XRD analysis after six recycling experiments. As presented in Fig. 9b, after six recycle photocatalytic processes, no obvious change was found from the XRD peaks of the recycled samples. The result indicated that the crystal structures of the heterojunction materials were not destroyed, suggesting its good reusability and stability.

3.5. Degradation of NOR in the raw natural water

To assess the efficiency of the photocatalytic process for NOR elimination in an actual matrix, an experiment was carried out in the raw surface water samples collected from the Jingmi diversion aquaduct (JMDA) in Beijing. Water quality parameters of the

JMDA were given in Table S1. Besides the photocatalytic degradation, direct photolysis was also observed in the natural water. Compared to the photocatalytic degradation rates in MQ water and tap water, the NOR degradation rate in JMDA water was significantly inhibited. As shown in Table 1, the rate constants of NOR in MQ water and tap water were 4.5- and 2.9-fold faster than in JMDA water. This finding indicated that the matrix (DOM and inorganic salts) of natural water competed with the light source and scavenge radicals, and hindered light transmission, resulting in a reduced photocatalytic rate. The effect of the degradation efficiencies under the backgrounds of bicarbonate was not obvious, which indicated that the decontamination efficiency of $BiOBr/Fe_3O_4$ was hardly influenced by its intrinsic properties, but could be affected mainly by other parameters such as nitrate, pH value, and dissolved organic matter.

3.6. The degradation products/intermediates

The degradation mechanism of NOR in the $BiOBr/Fe_3O_4$ system was investigated and a tentative transformation pathway was proposed. The NOR degradation mainly involved piperazine ring transformation (pathway I), decarboxylation (pathway II) and defluorination (pathway III) (Scheme 1). The piperazine ring cleavage played major roles in the photocatalytic degradation process, and the ${}^\bullet OH$ radical was the main reactive species in $BiOBr/Fe_3O_4$ catalytic system.

The degradation intermediates of NOR were shown in Table S2, and all products showed fragmentation patterns quite similar to that of NOR, with a common base structure-heterocyclic quinolone ring. Eleven intermediates were verified, and the detailed information about the degradation pathway was shown in Scheme 1. Firstly, NOR degradation was initiated by piperazine ring transformation (pathway I), followed by the sequential attack of ${}^\bullet OH$ radicals in piperazine ring, and generated compound A ($m/z = 336$) and B ($m/z = 350$). Here, the decarbonylation occurred in the amide (product B) under the inducement of ${}^\bullet OH$ radicals. The converted product at m/z 276 was consistent with the loss of CO_2, indicating the production of intermediate N with the decarbonylation by the pathway III. The intermediate product C was formed from hydroxyl oxidation. The intermediates at m/z 294 (D), 276 (G), 251 (E), 236 (F) and 233 (H) were also identified in previous literature [5,14,17,42]. The product D, E and F were obtained from the piperazine ring cleavage. The product D was likely to generate after product C due to the peak concentration for D appeared after a few seconds. From D → E, the amine with functional group of $-NH-(CH_2)_2-NH_2$ was oxidized and decaronylated to $-NH_2$, then the product E was produced. Compound G and H were produced through the pathway II with defluorination. Particularly, the products J (278) and M (192) were generated via the defluorination process, and the two compounds were for the first time detected and reported in this study. It also provided a vital evidence for the participation of hydroxyl radicals in the photocatalysis process in $BiOBr/Fe_3O_4$ system.

3.7. Toxicity evolvement

The toxicity of NOR and its degradation products during the irradiation were evaluated using the *V. fischeri* luminescent bacteria assay. Fig. 10 showed the evolution of toxicity (expressed as% inhibition) alongside the experiments. The luminescence inhibition rate of the parent NOR (0 min of irradiation) to *V. fischeri* was 50.2%, and with the irradiation time went on, the toxicity first slightly decreased to 27% at 10 min, then increased up to the highest of 55.6% at 30 min, implying the generation of some more toxic intermediates than the parent compound. LC–MS analysis showed that some degradation products were detected. These piperazine ring transformation and oxidation resulted in a lower steric resistance
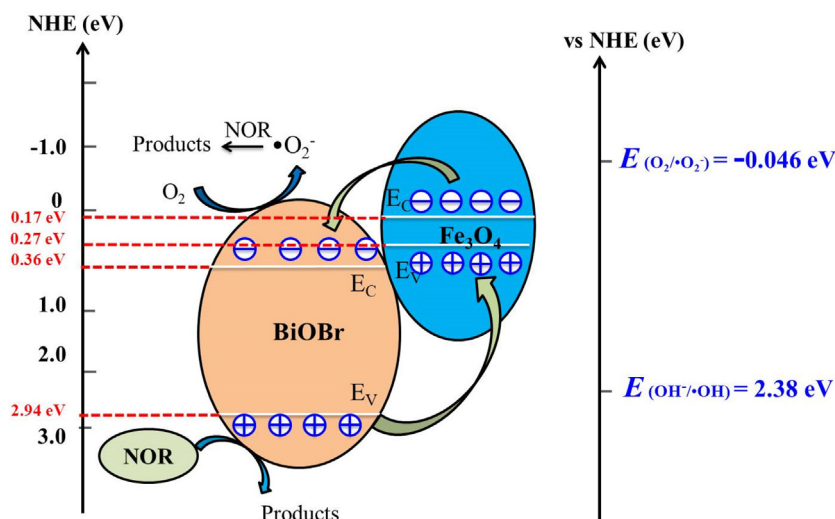
Fig. 8. Schematic diagram of electron-hole pairs separation and the possible reaction mechanism over BiOBr/Fe$_3$O$_4$ photocatalyst.
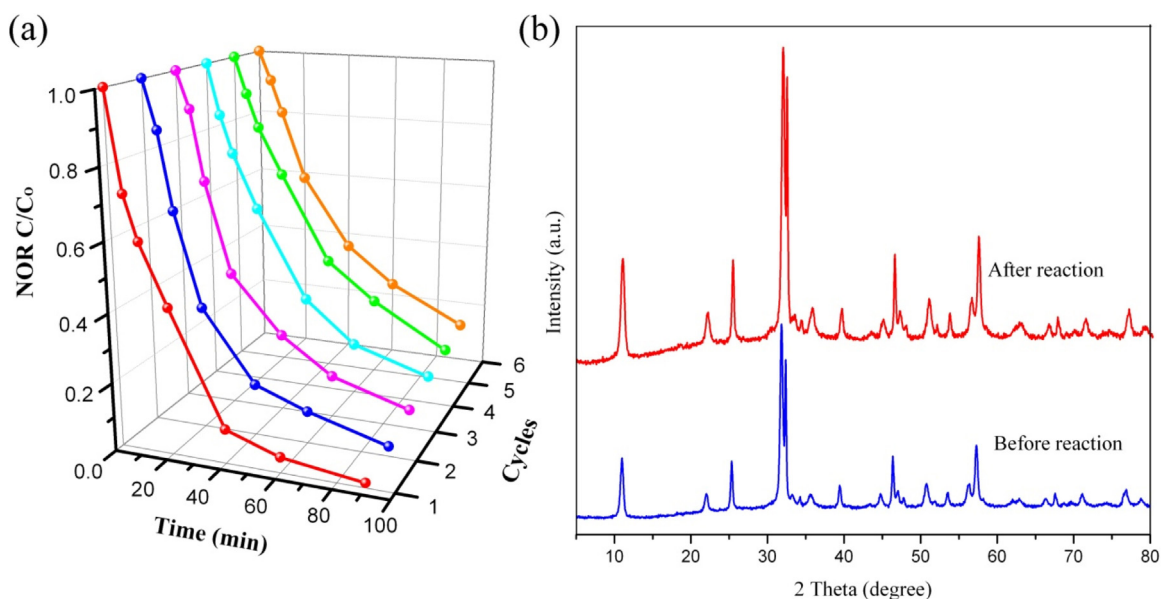

Fig. 9. (a) Recycle experiments for the NOR degradation by BiOBr/Fe$_3$O$_4$ under visible light irradiation; (b) XRD patterns of the BiOBr/Fe$_3$O$_4$ before and after six recycle photocatalytic degradation process.

Table 1
Measured degradation parameters of NOR by BiOBr/Fe$_3$O$_4$ in various water matrices.

matrix	degradation processes	NOR[a]	
		rate constant (min^{-1})	T$_{1/2}$ (min)[f]
MQ water	direct photolysis	0.0029	239.0
Methanol	photocatalytic degradation	0.0025	277.3
MQ water	photocatalytic degradation	0.0837	8.3
MQ + DOM[b]	photocatalytic with ^{3}DOM	0.0211	33.0
MQ+ bicarbonate[c]	photocatalytic with HCO$_3^-$	0.0871	7.9
MQ + nitrate[d]	photocatalytic with NO$_3^-$	0.0641	10.8
JMDA water[e]	photocatalytic degradation	0.0186	37.3
Tap water	photocatalytic degradation	0.0548	12.6

[a] Photocatalyst, 0.5 g L^{-1}; NOR, 10 mg L^{-1}, pH = 7.0 ± 0.2 unless otherwise indicated.
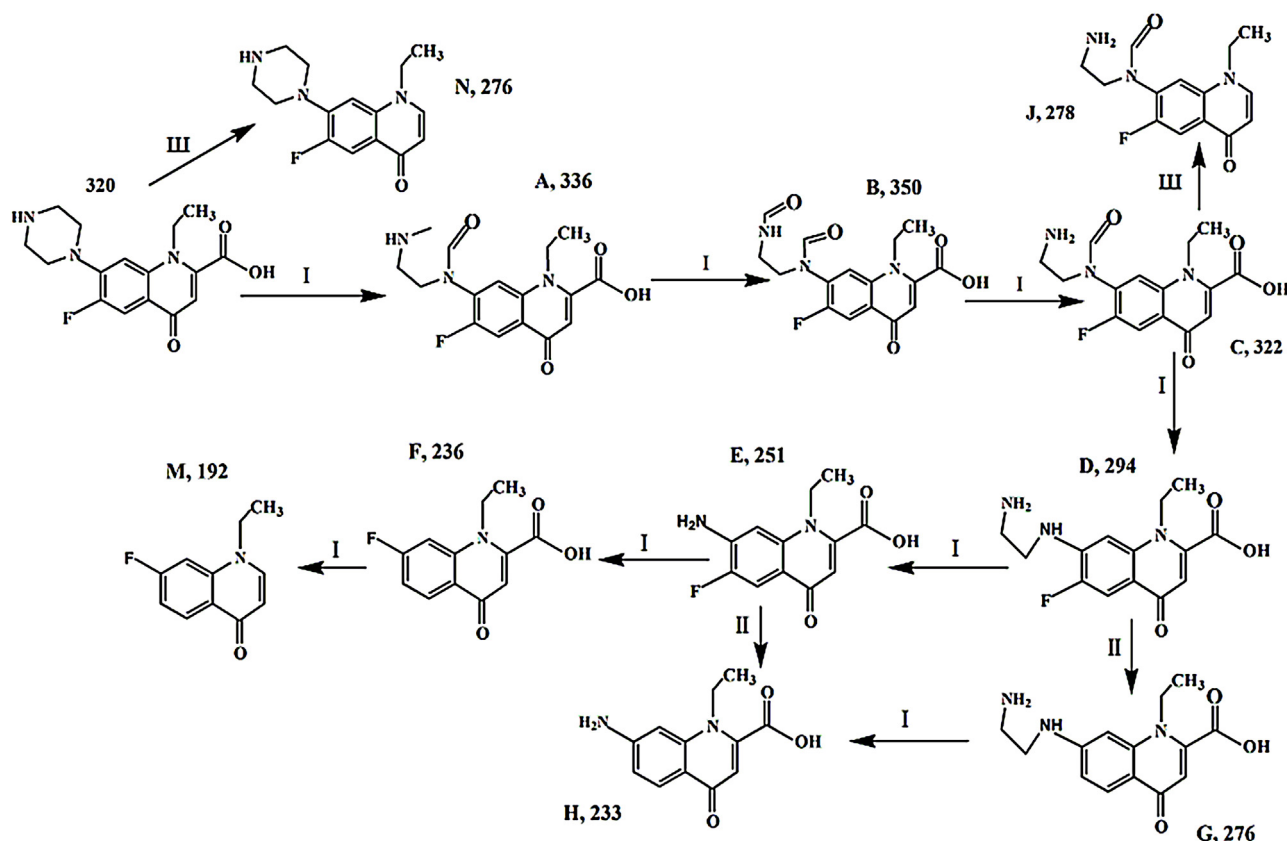[b] HA, representing DOM in this study, [HA] = 2.5 mM.
[c] [HCO$_3^-$] = 4.0 mM.
[d] [NO$_3^-$] = 1 mM.
[e] Water quality parameters shown in Table S1.
[f] T$_{1/2}$ = ln2/k.

Scheme 1. Proposed photocatalytic transformation pathways of NOR by BiOBr/Fe₃O₄.
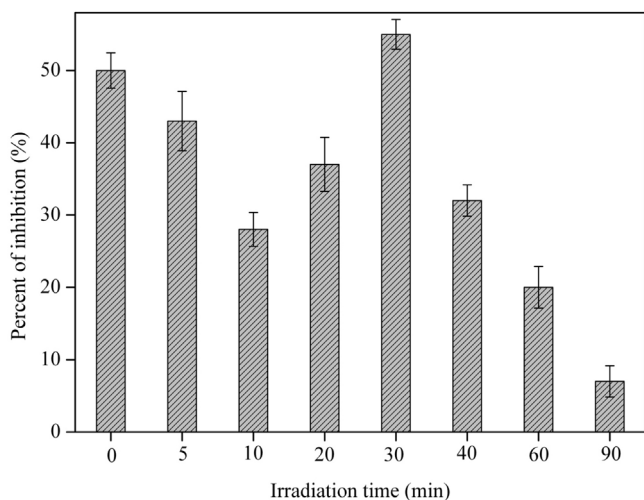

Fig. 10. Toxicity evolution of the photocatalytic degradation products using *V. fischeri* bioassays at pH = 7.08 and initial NOR concentration of 10 mg L^{-1}.

and an easier penetration into cell of luminescent bacteria, which subsequently led to the increase of toxicity [43,44]. As the reaction went on, the intermediates/products exerted lower toxicity to the bacteria, and after 90 min irradiation, 7% inhibition was observed. The result suggested that during the NOR removal through photocatalytic degradation, the ecotoxicological risk of NOR could be lowered or diminished.

4. Conclusions

In this work, the magnetic recoverable BiOBr/Fe₃O₄, synthesized by a facile in-situ co-precipitation method, was applied to the photocatalytic degradation of NOR. BiOBr/Fe₃O₄ heterogeneous catalysts exhibited a notable catalytic activity for NOR degradation. The maximum degradation of NOR in 0.5 g L^{-1} of BiOBr/Fe₃O₄ system could be attained within 30 min visible light irradiation at pH 9.0. The photocatalytic degradation followed a pseudo-first order reaction with rate constants of 0.076 min^{-1}. NOR degradation by BiOBr/Fe₃O₄ was enhanced with the increase of bicarbonate doses ranging from 0.5 to 4.0 mM. DOM inhibited the catalytic degradation in the range of 2.5–10 mM. Nitrate stimulated NOR degradation in the catalytic degradation at the concentration less than 1 mM but inhibited at 2.0–10 mM. Oxidation by superoxide radicals and hydroxyl radicals were the main mechanism of NOR degradation in BiOBr/Fe₃O₄ system. Based on the identification of products by HPLC–MS, the degradation pathways of NOR were proposed, which mainly involved the piperazine ring transformation, decarboxylation and defluorination to generate eleven intermediates. Toxicity assays by *Vibrio fischeri* proved that the NOR photocatalytic transformation products retained negligible antibacterial activity relative to the parent compound. Photocatalytic degradation of NOR by BiOBr/Fe₃O₄ was also effective in the raw natural water, which provided a reference for its real application.

Appendix A. Supplementary data

Supplementary data associated with this article can be found, in the online version, at http://dx.doi.org/10.1016/j.apcatb.2016.12.032.

Supplementary materials contain graph of the XPS spectrum of $BiOBr/Fe_3O_4$ sample, room-temperature magnetic hysteresis loops, N_2 adsorption-desorption isotherms of the as-synthesized samples, UV–vis diffuse reflectance spectra of BiOBr and $BiOBr/Fe_3O_4$, the UV–vis absorption spectra of NOR and the UV–vis spectrum of the HA, adsorption-desorption equilibrium of NOR in darkness, ESR spectra, the TOC changes, table of the characteristics of water sample from JMDA and the identified possible reaction intermediates of NOR under visible light irradiation, which are available to authorized users.

References

[1] S.-C. Kim, K. Carlson, Environ. Sci. Technol. 41 (2007) 50–57.
[2] B. Kasprzyk-Hordern, R.M. Dinsdale, A.J. Guwy, Water Res. 43 (2009) 363–380.
[3] V. Kitsiou, A. Antoniadis, D. Mantzavinos, I. Poulios, J. Chem. Technol. Biotechnol. 89 (2014) 1668–1674.
[4] X. Chang, M.T. Meyer, X. Liu, Q. Zhao, H. Chen, J.-a. Chen, Z. Qiu, L. Yang, J. Cao, W. Shu, Environ. Pollut. 158 (2010) 1444–1450.
[5] T. An, H. Yang, W. Song, G. Li, H. Luo, W.J. Cooper, J. Phys. Chem. A 114 (2010) 2569–2575.
[6] M. Chen, W. Chu, Ind. Eng. Chem. Res. 51 (2012) 4887–4893.
[7] Y. Xu, C. Guo, Y. Luo, J. Lv, Y. Zhang, H. Lin, L. Wang, J. Xu, Environ. Pollut. 213 (2016) 833–840.
[8] X.-H. Wang, A.Y.-C. Lin, Environ. Sci. Technol. 46 (2012) 12417–12426.
[9] Z. Ye, H.S. Weinberg, M.T. Meyer, Anal. Chem. 79 (2007) 1135–1144.
[10] Yiruhan, Q.-J. Wang, C.-H. Mo, Y.-W. Li, P. Gao, Y.-P. Tai, Y. Zhang, Z.-L. Ruan, J.-W. Xu, Environ. Pollut. 158 (2010) 2350–2358.
[11] R.A. Brain, D.J. Johnson, S.M. Richards, H. Sanderson, P.K. Sibley, K.R. Solomon, Environ. Toxicol. Chem. 23 (2004) 371–382.
[12] A.A. Robinson, J.B. Belden, M.J. Lydy, Environ. Toxicol. Chem. 24 (2005) 423–430.
[13] B. Li, T. Zhang, Environ. Sci. Technol. 44 (2010) 3468–3473.
[14] H. Zhang, C.-H. Huang, Environ. Sci. Technol. 39 (2005) 4474–4483.
[15] A. Fakhri, S. Behrouz, Sol. Energy 117 (2015) 187–191.
[16] M. Chen, W. Chu, J. Hazard. Mater. 219–220 (2012) 183–189.
[17] M. Chen, W. Chu, Appl. Catal. B: Environ. 168–169 (2015) 175–182.
[18] X. Li, C. Niu, D. Huang, X. Wang, X. Zhang, G. Zeng, Q. Niu, Appl. Surf. Sci. 286 (2013) 40–46.
[19] L. Zhang, W. Wang, L. Zhou, M. Shang, S. Sun, Appl. Catal. B: Environ. 90 (2009) 458–462.
[20] J. Xu, L. Li, C. Guo, Y. Zhang, S. Wang, J. Chem. Eng. 221 (2013) 230–237.
[21] C. Guo, Y. He, P. Du, X. Zhao, J. Lv, W. Meng, Y. Zhang, J. Xu, Appl. Surf. Sci. 320 (2014) 383–390.
[22] P. Calza, S. Marchisio, C. Medana, C. Baiocchi, Anal. Bioanal.Chem. 396 (2010) 1539–1550.
[23] T. Yamashita, P. Hayes, Appl. Surf. Sci. 254 (2008) 2441–2449.
[24] W.-H. Li, X.-P. Yue, C.-S. Guo, J.-P. Lv, S.-S. Liu, Y. Zhang, J. Xu, Appl. Surf. Sci. 335 (2015) 23–28.
[25] J. Xu, W. Meng, Y. Zhang, L. Li, C. Guo, Appl. Catal. B: Environ. 107 (2011) 355–362.
[26] I. Michael, E. Hapeshi, C. Michael, D. Fatta-Kassinos, Water Res. 44 (2010) 5450–5462.
[27] J.P. Hassett, Science 311 (2006) 1723–1724.
[28] D. Vione, G. Falletti, V. Maurino, C. Minero, E. Pelizzetti, M. Malandrino, R. Ajassa, R.-I. Olariu, C. Arsene, Environ. Sci. Technol. 40 (2006) 3775–3781.
[29] M. Zhan, X. Yang, Q. Xian, L. Kong, Chemosphere 63 (2006) 378–386.
[30] A.D. Dimou, V.A. Sakkas, T.A. Albanis, J. Photochem. Photobiol. A 163 (2004) 473–480.
[31] J. Xu, Z. Hao, C. Guo, Y. Zhang, Y. He, W. Meng, Chemosphere 99 (2014) 186–191.
[32] J. Suzuki, T. Sato, A. Ito, S. Suzuki, Chemosphere 16 (1987) 1289–1300.
[33] C. Wang, L. Zhu, M. Wei, P. Chen, G. Shan, Water Res. 46 (2012) 845–853.
[34] P. Mazellier, C. Busset, A. Delmont, J. De Laat, Water Res. 41 (2007) 4585–4594.
[35] M.W. Lam, K. Tantuco, S.A. Mabury, Environ. Sci. Technol. 37 (2003) 899–907.
[36] D. Vione, S. Khanra, S.C. Man, P.R. Maddigapu, R. Das, C. Arsene, R.-I. Olariu, V. Maurino, C. Minero, Water Res. 43 (2009) 4718–4728.
[37] J. Huang, S.A. Mabury, Chemosphere 41 (2000) 1775–1782.
[38] A.L. Teel, C.R. Warberg, D.A. Atkinson, R.J. Watts, Water Res. 35 (2001) 977–984.
[39] H. Fang, Y. Gao, G. Li, J. An, P.-K. Wong, H. Fu, S. Yao, X. Nie, T. An, Environ. Sci. Technol. 47 (2013) 2704–2712.
[40] G.K. Pradhan, S. Martha, K.M. Parida, ACS Appl. Mater. Interfaces 4 (2012) 707–713.
[41] S. Shenawi-Khalil, V. Uvarov, S. Fronton, I. Popov, Y. Sasson, J. Phys. Chem. C 116 (2012) 11004–11012.
[42] T. Paul, M.C. Dodd, T.J. Strathmann, Water Res. 44 (2010) 3121–3132.
[43] Y. Li, J. Niu, W. Wang, Chemosphere 85 (2011) 892–897.
[44] S. Jiao, S. Zheng, D. Yin, L. Wang, L. Chen, Chemosphere 73 (2008) 377–382.